Published in final edited form as:

Biotechnol Bioeng. 2016 October ; 113(10): 2264–2274. doi:10.1002/bit.25987.

Microcapsules and 3D Customizable Shelled Microenvironments From Laser Direct-Written Microbeads

David M. Kingsley,

Andrew D. Dias,

David T. Corr

Department of Biomedical Engineering, Rensselaer Polytechnic Institute, 110 Eighth St., Troy, New York 12180;

Abstract

Microcapsules are shelled 3D microenvironments, with a liquid core. These core-shelled structures enable cell–cell contact, cellular proliferation and aggregation within the capsule, and can be utilized for controlled release of encapsulated contents. Traditional microcapsule fabrication methods provide limited control of capsule size, and are unable to control capsule placement. To overcome these limitations, we demonstrate size and spatial control of poly-L-lysine and chitosan microcapsules, using laser direct-write (LDW) printing, and subsequent processing, of alginate microbeads. Additionally, microbeads were used as volume pixels (voxels) to form continuous 3D hydrogel structures, which were processed like capsules, to form custom shelled aqueous-core 3D structures of prescribed geometry; such as strands, rings, and bifurcations. Heterogeneous structures were also created with controlled initial locations of different cell types, to demonstrate the ability to prescribe cell signaling (heterotypic and homotypic) in co-culture conditions. Herein, we demonstrate LDW's ability to fabricate intricate 3D structures, essentially with "printed macroporosity," and to precisely control structural composition by bottom-up fabrication in a bead-by-bead manner. The structural and compositional control afforded by this process enables the creation of a wide range of new constructs, with many potential applications in tissue engineering and regenerative medicine.

Keywords

alginate; laser direct-write; micropatterning; microstrand; microcapsule; microbead

Introduction

Many state-of-the-art applications in tissue engineering and in vitro diagnostics employ encapsulation and printing technologies, often based on the use of hydrogels (Dias et al., 2015). However, conventional bulk hydrogel encapsulation suffers from limited nutrient and waste exchange (Griffith et al., 2005), as well as poor spatial control of hydrogel

Correspondence to: D.T. Corr, telephone: (518) 276-3276; fax: (518) 276-3035; corrd@rpi.edu.

The authors have no conflicts of interest to declare.

constituents and payload (Dias et al., 2015). Unfavorable hydrogel diffusion kinetics can lead to necrosis of encapsulated cells, once the thickness exceeds the diffusion limit of the hydrogel (Freed et al., 1994). To address these diffusion and mass transport limitations, microbead geometries are often utilized for culturing cells. While these hydrogel microbeads provide a 3D cellular environment, with the favorable surface-to-volume ratio of a spherical geometry, the lack of spatial control limits the study of localized signaling, complex microenvironments, and directional cellular interactions. Recently, we have demonstrated a method to fabricate and pattern microbeads in a single step (Kingsley et al., 2013), enabling spatial patterning of size-controlled microbeads.

Despite the geometric advantages of microbeads, approaches utilizing hydrogels such as alginate do not allow normal cell proliferation and growth, as would be seen in native (or natural) extracellular matrix (ECM). This change in cell functionality can be attributed to the absence of many key features of the native ECM, such as cell attachment sites, macroporosity, and enzymes necessary for matrix degradation. While prior studies have modified the hydrogel matrix by adding select ECM components to produce hydrogel blends (e.g., (Yao et al., 2013)), or grafting cell binding sequences (e.g., RGD) to enhance cell function (e.g., (Bidarra et al., 2010)), other work further processes microbeads into microcapsules to provide 3D environments to allow cell–cell contact without limiting cell functionality.

Microcapsules are spherical microstructures, consisting of a semipermeable shell surrounding an aqueous core (Lim and Sun, 1980). In contrast to microbeads, cells encapsulated in microcapsules grow and proliferate on the interior shell surface (Wang et al., 2006a), and must produce matrix and/or self-assemble into aggregates to grow in 3D (Zhang et al., 2005). Typically, microcapsules are fabricated through the processing of microbeads, by coating charged hydrogel microbeads with a polymer of opposite charge (Hernández et al., 2010) (e.g., a negatively charged alginate microbead and positively charged poly-L-lysine (PLL) or chitosan). This process forms a shell in a phenomenon known as polyelectrolyte complexation (Gåserød et al., 1998; Thu et al., 1996a). The interior of the bead can then be solubilized by using a reverse crosslinking agent (Gåserød et al., 1998). The resulting structure is a shell retaining the microbead payload in an aqueous core. Microcapsules have been characterized (Gåserød et al., 1999; Thu et al., 1996b) and utilized for numerous in vitro applications (Raof et al., 2011a; Rokstad et al., 2011).

However, current microbead/microcapsule fabrication approaches are limited due to their lack of control over bead, and thus microcapsule, spatial position. As such, these techniques cannot control microcapsule patterning to prescribe and study modes of cellular signaling (i.e., juxtacrine, paracrine). It would also be beneficial if the bio-payload could be localized, so that cellular heterogeneity and geometric complexity could be introduced into core-shelled microstructures.

Herein, we demonstrate the ability to process laser-fabricated and patterned alginate microbeads into either alginate-chitosan or alginate-PLL microcapsules. Capsules maintained a viable cellular payload (e.g., MDA-MB-231 cancer cells), and maintain initial pattern fidelity. We further show that microbeads can be patterned in partially overlapping

arrangements to create continuous 3D structures (e.g., microstrands, bifurcations, and rings). These structures were processed with either chitosan or PLL to produce 3D shelled microstructures, of user-defined geometry. As such, the geometry, composition, and size of these microstructures were prescribed at the level of individual microbeads, which were used as volume pixels (voxels). This enables the creation of continuous, shelled 3D microenvironments, in which the initial position of the biopayload, including cells of various types and other biologics (e.g., proteins, growth factors), is controlled, and the structure is allowed to evolve with time. Such compositional and positional control offers the placement of macroporosity (i.e., large pores allowing cell migration and proliferation, in contrast with the microporous structure of hydrogels that only allow diffusion). Other benefits of this approach include unrestricted cell growth, structural evolution, and spatial precision of construct payload, unrealized by traditional tissue engineering and biofabrication techniques.

Materials and Methods

Cell Culture—MDA-MB-231 and Fibroblasts

GFP-labeled MDA-MB-231-gfp (M231) human breast cancer cells (ATCC, Manassas, VA) were grown in standard cell culture conditions (37°C, 5% CO_2, 95% RH) in growth medium consisting of Dulbecco's Modified Eagle's Medium (DMEM) supplemented with 10% (v/v) fetal bovine serum (FBS), 100 U/mL penicillin/streptomycin, and 2 mM L-glutamine. Normal human lung fibroblasts (Lonza) labeled using RFP lenti-viral transfection, were cultured in DMEM supplemented with 10% (v/v) FBS and 100 U/mL penicillin/streptomycin.

Laser-Based Microbead Fabrication

We previously describe a method of single-step laser-based alginate microbead fabrication and patterning (Kingsley et al., 2013). Briefly, a LDW system (Schiele et al., 2011) is utilized, consisting of two parallel stages, the top being the print ribbon stage, and the bottom the receiving substrate (Fig. 1). The ribbon is a UV-transparent quartz disk (Edmund Optics, Barrington, NJ) with the underside coated with a thin sacrificial layer and the transfer material. In this study, a spin-coated thin film of 10% gelatin/2% alginate served as the sacrificial layer, and cells suspended in 2% alginate comprised the transfer material. To prepare the receiving substrate, a Petri dish was spin-coated with a thin layer of 10% gelatin and 2% calcium chloride ($CaCl_2$), and washed with 2% $CaCl_2$. A microbead is fabricated by a single pulse from an ArF excimer laser (Teosys LLC, Crofton, MD; λ = 193 nm) that volatilizes the sacrificial layer on the ribbon, ejecting a droplet of transfer material to the receiving substrate (Fig. 1a). During printing, the gelatin on the substrate provides a thin viscous layer to cushion and immobilize the transfer material, whereas the Ca^{2+} rapidly crosslinks with alginate, encapsulating the cellular payload in an immobilized, size-controlled 3D microbead.

After bead deposition, the independent x-y Computer-Aided Design/Computer-Aided Manufacturing (CAD-CAM)-controlled motorized stages moved to the next target spot for additional bead deposition. Upon completing the transfer pattern, the receiving dish containing the cell-loaded alginate microbeads was incubated for 10 min.

Processing Microbeads to Chitosan- and PLL-Shelled Microcapsules

Two slightly different methods were used for creating PLL or chitosan microcapsules, based on previously established methods (Wang et al., 2006b) (schematically represented in Fig. 1). All washes were 1 mL for 10-cm-diameter Petri dishes, regardless of the number of patterns per dish. To create PLL microcapsules, after the fabrication of alginate beads, the receiving substrate was washed once with 300 mM mannitol/25 mM HEPES to remove calcium chloride solution, then incubated with 0.1% (w/v) PLL solution/300 mM mannitol/25 mM HEPES while rocking for 5 min to allow for polyelectrolyte complexation between the polyanionic alginate beads and polycationic PLL. Dishes were washed once again with 300 mM mannitol/25 mM HEPES, to remove the complexing agent, and then washed with 0.15% alginate/0.85% NaCl to provide additional stabilization. To liquefy the bead cores, 1.6% (w/v) sodium citrate solution was added to dishes for 2 min to chelate the calcium crosslinking the alginate. The sodium citrate was removed with a wash (300 mM mannitol/25 mM HEPES). The resulting 3D microcapsules have cells in a liquid core that is contained by the alginate and PLL-complexed shells. Following fabrication, fresh media was added, and the printed capsules were maintained in culture.

Similar to the PLL process, to fabricate chitosan microcapsules, microbeads were incubated for 1 h after transfer. Media was removed, and capsules were washed thrice with 0.85% NaCl. Beads were incubated in 0.5% chitosan for 7 min with rocking, to create the alginate–chitosan shell complex around the bead, then washed again with 0.85% NaCl to removed excess chitosan, and incubated for 2 min in sodium citrate to liquefy the cores. Finally the citrate was removed, and replaced with culture media for the M231 cells.

PLL and Chitosan Microcapsule Pattern Registry and Size

Pattern registry and size of microbeads and microcapsules were analyzed using ImageJ (Rasband, 2004). Images were modified for analysis using the processes “enhance contrast,” and then converted to binary. The “fill hole” function was then applied (if necessary, “dilation” and “close” functions were also used) resulting in the final image being black masks of the microbead or microcapsule with a white background. Finally, the “analyze particle” tool was used to determine the diameter and coordinates of the centroid for each of the masked positions. Centroid-to-centroid distances of microcapsule arrays were compared to their respective microbead arrays to identify any changes in pattern registry with processing. All measurements regarding pattern registry were made using an image analysis algorithm to identify centroid locations and distances. This substantially reduces bias, and we detail this algorithm above. Measurements were taken immediately after printing, and immediately after processing to microcapsules (coating with either a chitosan or PLL and subsequent chelation).

PLL and Chitosan Microcapsule Viability Assay

Cell viability within PLL and chitosan microcapsules was determined using a Live-Dead Staining Kit (Enzo Life Sciences, Farmingdale, NY), following manufacturer’s directions. Viability was assessed at 1 h, 3 days, and 5 days after capsule fabrication; live cells stain green and dead cells (cells with compromised membranes) stain red.

Multichannel fluorescent and phase-contrast imaging was performed using a Zeiss Z1 microscope using Axiovision software (Carl Zeiss, Thornwood, NY). Live-dead imaging was performed on 3 × 4 microcapsule arrays. The numbers of red and green cells in each channel were counted separately, and the average cell viability was calculated at each timepoint as an overall percentage.

Statistical Analysis

For pattern registry analysis, all patterns were composed of 3 × 4 microbead arrays, and their corresponding microcapsule arrays, with $n = 3$. The relative centroid-to-centroid distances of the sample arrays were pooled into 4 groups: pre-chitosan microbeads, chitosan microcapsules, pre-PLL microbeads, and PLL microcapsules. To determine if processing into microcapsules affected pattern registry, a paired-sample t-test compared chitosan and PLL microcapsules to their respective pre-coated group (pre-chitosan microbeads or pre-PLL microbeads). Differences in which $P < 0.05$ were considered statistically significant.

Viability scores for each condition and time were based upon the average of three independent 3 × 4 microcapsule arrays. Sample means were compared using one-way analysis of variance (ANOVA), and Tukey's Honestly Significant Difference post hoc test with R Statistical Software (Team, 2014), to identify any significant differences. Differences in which $P < 0.05$ were considered statistically significant.

Microstrand and Complex Geometry Fabrication

Microstrands utilize the same setup as previously described for microcapsules. To start, microbeads were printed in partially overlapping fashion, in custom pattern geometries, to create a continuous 3D hydrogel structure. This entire structure was then shelled with a polymer (e.g., PLL or chitosan), and the core was liquefied via chelation, as previously described for microcapsules. This resulted in a continuous structure, in which the cells (or other biopayload) were in an aqueous core, constrained by the solid polymeric shells.

Confocal Imaging of Microcapsules

To visualize the 3D structure of cellular aggregates within chitosan microcapsules, alginate beads were printed to 30 mm coverslips and processed to microcapsules as previously described. Cells were allowed to grow for 7-days within the microcapsule, then the microcapsule samples were washed twice with Dulbecco's phosphate-buffered saline (DPBS) and fixed with 4% Paraformaldehyde, followed by two additional DPBS washes. To visualize nuclei, cells were incubated with 0.1 μg/mL DAPI (4′,6-diamidino-2-phenylindole) solution for 5 min, and washed again with PBS. Samples were stored in PBS at 4°C until imaging. Confocal imaging was performed with a Zeiss LSM510 META-NLO laser scanning microscope system (Albany, NY). Images were acquired with a 63× oil immersion lens. To visualize the 3D cellular aggregate within a microcapsule, vertical sections were taken with the z-stack function to produce an overall 3D rendering.

Results

Patterned Microcapsule Fabrication and Characterization

Laser direct-written microbeads were successfully processed into microcapsules with both PLL and chitosan coatings. Proliferating cells were observed in both types of microcapsules over a 7-day period (Fig. 2). By day 7, cells had proliferated to fill the microcapsules, in both PLL and chitosan microcapsules. There were observable differences in morphology between cells grown inside PLL and chitosan capsules: cells in the PLL microcapsules adopted a more spread morphology, while those within chitosan capsules exhibited little to no spreading, appearing morphologically spherical. Additionally, it appears that microcapsules made from PLL shrunk in size, compared to that of the original bead.

Next, we examined the structure of cellular aggregates within microcapsules after 7-days of growth. The aggregates exhibited cells present in multiple vertical planes, suggesting a 3D structure within the microcapsule. We further confirmed the 3D structure with z-stack confocal imaging. For example, an orthogonal view of DAPI stained GFP-expressing M231 cells within a microcapsule shows the cellular aggregate at 7 days of growth is spheroidal in shape, and approximately 80 μm in the z-direction (Fig. 3).

Microcapsule Pattern Registry and Size

The pattern registry before and after the application of the polycationic coating (PLL or chitosan) was analyzed to determine if the coating procedure significantly disrupted the print pattern. Microbead arrays with controlled spacing were fabricated according to a program that prescribed 600-μm centroid-to-centroid spacing (Fig. 4). Image analysis identified the average centroid-to-centroid spacing between fabricated microbeads within the arrays to be used for either PLL (612.9 ± 21.4 μm) or chitosan (588.8 ± 22.8 μm) coating (Table I). When further processed into microcapsules, by polymeric coating and subsequent chelation, the relative centroid-to-centroid distance changed by 8.1 ± 7.8 μm (1.4 ± 1.3%) for PLL, and 9.9 ± 8.6 μm (1.7 ± 1.4%) for chitosan. No significant difference was seen in the mean centroid-to-centroid distances for both chitosan and PLL microcapsule groups compared to their corresponding pre-coated microbead group, indicating no detectable change in pattern registry with processing into microcapsules.

To determine if the coating procedure impacted microcapsule size, the diameter of microbeads in the pre-coated group (chitosan or PLL) was compared with that of the corresponding microcapsule group. When processed from alginate microbeads, the diameter of chitosan microcapsules increased by 28.5 ± 8.5%, whereas the diameter of PLL microcapsules decreased 6.5 ± 4.5%, on average (Table I).

Cell Viability in PLL and Chitosan Microcapsules

Short-term (1 h) and longer-term (3 days, 5 days) cell viability was assessed within chitosan and PLL capsules to identify any differences in viability due to the coating procedures or the material of the shell coating. Cell viability within PLL and chitosan capsules was reported 1 h, 3 days, and 5 days after processing (Fig. 5). ANOVA revealed that the average number of living cells increased with time for both coatings, and was higher in chitosan capsules than

PLL ($P < 0.01$). There was no evidence of a time-coating interaction influence on viability. Tukey HSD identified that chitosan capsules had an average viability 16.3% higher than that of PLL, with significantly greater viability than PLL capsules at each time point.

Microstrand Fabrication

Long, aqueous core, microstrands were successfully fabricated by rapidly printing overlapping beads, then applying either chitosan or PLL, and liquefying the core using the calcium chelator sodium citrate. The result appeared to be a continuous cylindrical thin-walled vessel structure, or microstrand, which constrained cell migration within the strand volume. Alginate-chitosan microstrands were initially loaded with only M231 cells, which appeared to completely fill strands over 9 days (Fig. 6). M231 cells again did not appear to spread as they attach to chitosan-coated microenvironments, and remain in a spherical morphology. Some rupturing of microstrands was observed.

M231/fibroblast microstrand co-cultures were also fabricated to demonstrate the spatial control of the cellular payload within these continuous structures. Custom microstrands were created in which the initial composition was spatially prescribed, using two separate configurations: (i) one half of the strand containing M231 cells, and the other containing fibroblasts (Fig. 7a); and (ii) the strand compositionally broken into thirds, with fibroblasts in the central third, and M231 cells at either end (Fig. 7b), illustrating the ability to control or prescribe spatial heterogeneity within microstrands.

Additional Complex Strand Geometries

Custom programs were written to create more complex geometries using bead-by-bead microstrand fabrication. A bifurcated strand was successfully fabricated and filled with proliferating cells over a time period of 10 days (Fig. 8). Further, circular ring microstructures were also created to demonstrate the ability to fabricate a closed, continuous structure (Fig. 8). Cell growth and proliferation were continuous within the structures, suggesting continuity within the custom geometries.

Discussion

Bottom-up tissue engineering techniques, such as bioprinting and microfabrication, offer control of cellular placement within a construct. However, most bottom-up approaches utilize hydrogels as a support matrix, where the cells must break down the hydrogel, and proliferation may take a much longer time, often up to months (Zhu and Marchant, 2011). In this study, we have shown the capability of LDW-patterned microbeads to be processed into microcapsules and complex microstrands, with defined payload geometry and localization. The cores of these constructs are aqueous, allowing cell-cell contact, rapid cellular proliferation and 3D aggregation—filling the structures within a week. We used PLL and chitosan to demonstrate the capability of creating a polymer shell around a custom printed construct, essentially “printing macroporosity” using this method. In contrast, we previously found that while cells had high viability (89.7% at day 1) within LDW alginate microbeads, they were unable to proliferate or aggregate within the alginate

matrix (Kingsley et al., 2013). This is likely due to the cell's inability to interact with the alginate matrix (Rowley et al., 1999).

While microcapsules have been fabricated from PLL or chitosan in previous literature, never before have they been patterned onto a surface with precise size and spatial control, nor with single-bead resolution. Control over capsule size and placement follows from control over microbead size and localization, previously reported to be controllable within 8% and 2%, respectively, by LDW (Kingsley et al., 2013). Size-controlled depots of high cellularity may enable the creation of in vitro models of clustered cells, with defined localized delivery, or immobilized cellular nodes within a construct, potentially with multiple cell types. In this study, we found that initially patterned microbeads have placement controllable within 2% (agreeing with previous results (Kingsley et al., 2013)), and further processing into microcapsules increases this placement variability by approximately 1–1.5%. The increased variability could be due to minor changes in the shape and/or size of the microcapsule after coating, causing a slight shift in the location of the centroid. Additionally, we found that microbeads experience a change in diameter when processed into microcapsules with either chitosan or PLL, agreeing with results in the literature (Liu et al., 2004). In our experiments, chitosan-shelled microcapsules increased in diameter by approximately 29%, while those shelled with PLL decreased approximately 6.5%. While not directly examined herein, this change in diameter could be due to swelling or shrinking associated with differences in the osmolarity of the chitosan and PLL solutions used in the coating procedure (Liu et al., 2004; Thu et al., 1996b).

To demonstrate versatility of this method, PLL and chitosan were employed as polymeric coatings, because they represent two common materials utilized in tissue engineering. While both materials successfully formed continuous shell coatings, cell viability was higher in chitosan microcapsules, suggesting that it may produce more rapid filling of the construct interior, and may be superior to PLL when a rapid turnaround is desired. The lower cell viability within PLL microcapsules than those microcapsules shelled by chitosan indicates a different cellular response during processing from microbead to microcapsule. While not directly investigated in this study, the primary reason is likely due to the cytotoxicity of soluble PLL (prior to complexation with alginate) (Fischer et al., 2003). Previous literature has shown that viability within microcapsules is inversely proportional to coating time, implying there is a temporal effect of soluble PLL on viability (Machluf, 2006). Conversely, there is a cytotoxic aspect of the chitosan shelling procedure, as the chitosan solution is at a mildly acidic pH (approximately 6.2). However, determining the cause of the observed viability differences between the polymeric shells was beyond the scope of this study, and would require further investigation.

Additionally, there appeared to be morphological differences in M231 cells grown within shelled microenvironments of the two materials. Cells grown within the chitosan shell exhibited a more rounded morphology compared to those within the PLL environment. This suggests that even though the polycation is on the outer surface of the shell, there is a degree of penetration and exposure of charged residues with which the cells can interact, potentially making one coating more advantageous for adherent cells. Conversely, there may be a benefit to modifying the interior surface chemistry of microcapsules. One way this

might be achieved is by conjugating peptide sequences (e.g., RGD motif) to the alginate, so that these binding sites are exposed on the interior surface on the capsule.

We leveraged the precise microbead patterning ability of LDW to print size-controlled microbeads, in overlapping fashion, to create continuous 3D structures. The integrity of these structures was maintained throughout the shelling process, enabling creation of cell-laden geometries that are unachievable by other conventional fabrication techniques. Some of these structures had observable leaking that was attributed to osmotic stress. In other cases, leaking occurred after a period of culture where cells were able to exert sufficient force to disrupt the capsule structure. Encapsulated cells were able to grow in all parts of these aqueous-shelled structures, showing the continuity of the internal environment, and the absence of any occlusions. Further, these structures could be loaded with multiple cell types at desired locations, which can be applied in the future to perform complex co-culture or migratory studies. This spatial control enables specification of the interface at which different cell types interact in heterotypic co-culture, with the added benefit of a 3D microenvironment. Spatial complexity can be prescribed by including different biopayloads in microbead voxels along the structure, potentially allowing recapitulation of some aspects of in vivo complexity, all of which is not easily achievable by other technologies.

While continuous microstrands have been previously created using molds and continuous-flow electrostatic bead generators (Raof et al., 2011b; Unser et al., 2016), these techniques do not provide control over the location of suspended constituents. Microfluidic techniques are also able to load multiple cell types in channels, but flow-based techniques would face great difficulty when attempting to localize different cell types within a complex structure. This challenge is easily overcome using LDW. By processing LDW-printed overlapping alginate bead patterns into continuous structures, one end of a microstrand, or fork of a bifurcation, could have a different prescribed cellular composition than the other, with defined spatial locations of both cell types at any point in the structure. Furthermore, LDW printing of cell-containing alginate voxels could be used to create channels within gel systems. These alginate voxels could be liquefied with a calcium chelator to create a cell-lined channel, and flow could be introduced using microperfusion, to allow the influence of flow to be studied in a system in which the cells type(s) and initial location are prescribed.

There are many applications that could leverage this ability to produce geometrically customizable shelled-aqueous environments, with micron-level fabrication resolution, such as 3D cell migration studies, creating cellular gradients in defined geometries, and in vitro tissue models with complex cell–cell interactions. Individual microcapsules have recently been investigated for building tumor models in vitro that could be used for drug screening and other medical diagnostic tests (LaBarbera et al., 2012; Sakai et al., 2012; Zaytseva-Zotova et al., 2011). Tumor cells grown within microcapsules have shown the ability to aggregate and self-assemble to form 3D structures (Alessandri et al., 2013). Since cells grown in capsules have a drug response closer to that of an in vivo tumor than do those grown in 2D (Zhang et al., 2005), the patterning capabilities afforded by LDW may further lead to improved 3D cancer models. With the added ability to pattern microcapsules while controlling their contents, new models can be created where capsules of different cell types of the tumor (e.g., stromal cells and cancer cells) are placed within defined proximity, or

encapsulated together, to allow independent control of the mode of cellular signaling (i.e., paracrine or juxtracrine) within models.

Continuous structures fabricated by this method have numerous applications in tissue engineering. The confined geometry of strands, rings and bifurcations, and unrestricted cell growth within, enables directional migration assays, trans-capsule assays, chirality studies, and fabrication of structurally relevant organoids. Shelled, multi-bead structures, such as strands and bifurcations of different sizes could be fabricated to encapsulate fibroblasts, endothelial, and smooth muscle cells to create blood vessel structures with functional lumens. Such structures could prove useful for in vivo applications in tissue engineering and drug delivery. Furthermore, this enabling technology could potentially be applied to other polyelectrolyte materials, geometric structures, and cell types, providing a robust and versatile platform for tissue engineering research.

Conclusion

We have developed a method for fabricating chitosan and poly-l-lysine microcapsules in precise patterns, by combining LDW with previously existing capsule fabrication techniques. Cells inside of microcapsules proliferate in the constrained geometry, producing their own matrix and aggregating in 3D to fill the entire volume. This fabrication technique was further adapted to create continuous 3D structures, such as microstrands, bifurcations, and rings, in which the architecture and composition can be prescribed at the individual-microbead level. Thus, heterogeneous structures can be created, with different cell types at specific locations. This was demonstrated using GFP-M231 cells and RFP-Fibroblasts, to highlight this technology's capability to print cells at different initial positions in a constrained 3D geometry. Such functionality can enable new model development for fundamental cell and cell-signaling studies. The ability to pattern and prescribe the constituents of single microcapsules, or of continuous microstructures, provides potential to realize new in vitro tissue models. Further, this LDW-based fabrication technique is built on a CAD/CAM platform, allowing automation and scale-up of this technology to meet the demands of high-throughput applications.

Acknowledgments

This work was supported, in part, by funding from FA9550-11-C-0028 awarded by DoD, Air Force Office of Scientific Research, National Defense Science and Engineering Graduate (NDSEG) Fellowship, 32 CFR 168a (ADD), and NIH R56-DK088217 (DTC). The Xie lab (SUNY College of Nanoscale Science and Engineering) kindly provided M231 cells, and the Dai lab (Rensselaer Polytechnic Institute) kindly provided fibroblasts. The Barrasso lab (Albany Medical College) performed the confocal microscopy. We also acknowledge Sahir Jaggi for his contributions to protocol optimization.

Contract grant sponsor: NDSEG Graduate Research Fellowship (fellowship number 32 CFR 168a) from the Air Force Office of Scientific Research, within the Department of Defense (DoD)

Contract grant number: FA9550-11-C-0028

Contract grant sponsor: NIH

Contract grant number: R56-DK088217

References

Alessandri K, Sarangi BR, Gurchenkov VV, Sinha B, Kießling TR, Fetler L, Rico F, Scheuring S, Lamaze C, Simon A, Geraldo S, Vignjevic D, Doméjean H, Rolland L, Funfak A, Bibette J, Bremond N, Nassoy P. 2013. Cellular capsules as a tool for multicellular spheroid production and for investigating the mechanics of tumor progression in vitro. Proc Natl Acad Sci 110:14843–14848. http://www.pubmedcentral.nih.gov/articlerender.fcgi?artid = 3773746&tool = pmcentrez&rendertype = abstract [PubMed: 23980147]

Bidarra SJ, Barrias CC, Barbosa MA, Soares R, Granja PL. 2010. Immobilization of human mesenchymal stem cells within RGD-grafted alginate microspheres and assessment of their angiogenic potential. Biomacromolecules 11:1956–1964. [PubMed: 20690708]

Dias AD, Kingsley DM, Corr DT. 2015. Engineering 2D and 3D cellular microenvironments using laser direct-write. In: Grace L, Fisher J, Leong K, editors. 3D bioprinting nanotechnology in tissue engineering and regenerative medicine. London, UK: Elsevier. p 105–127.

Fischer D, Li Y, Ahlemeyer B, Krieglstein J, Kissel T. 2003. In vitro cytotoxicity testing of polycations: influence of polymer structure on cell viability and hemolysis. Biomaterials 24:1121–1131. http://www.ncbi.nlm.nih.gov/pubmed/12527253 [PubMed: 12527253]

Freed LE, Marquis JC, Langer R, Vunjak-Novakovic G. 1994. Kinetics of chondrocyte growth in cell-polymer implants. Biotechnol Bioeng 43:597–604. [PubMed: 18615759]

Gåserød O, Sannes A, Skjåk-Bræk G. 1999. Microcapsules of alginate-chitosan. II. A study of capsule stability and permeability. Biomaterials 20:773–783. [PubMed: 10353660]

Gåserød O, Smidsrød O, Skjåk-Bræk G. 1998. Microcapsules of alginate-chitosan-I: A quantitative study of the interaction between alginate and chitosan. Biomaterials 19:1815–1825. [PubMed: 9855182]

Griffith CK, Miller C, Sainson RCA, Calvert JW, Jeon NL, Hughes CC, George SC. 2005. Diffusion limits of an in vitro thick prevascularized tissue. Tissue Eng 11:257–266. [PubMed: 15738680]

Hernáandez RMA, Orive G, Murua A, Pedraz JL. 2010. Microcapsules and microcarriers for in situ cell delivery. Adv Drug Deliv Rev 62:711–730. http://www.ncbi.nlm.nih.gov/pubmed/20153388 [PubMed: 20153388]

Kingsley DM, Dias AD, Chrisey DB, Corr DT. 2013. Single-step laser-based fabrication and patterning of cell-encapsulated alginate microbeads. Biofabrication 5:045006. [PubMed: 24192221]

LaBarbera DV, Reid BG, Yoo BH. 2012. The multicellular tumor spheroid model for high-throughput cancer drug discovery. Expert Opin Drug Discov 7:819–830. [PubMed: 22788761]

Lim F, Sun AM. 1980. Microencapsulated islets as bioartificial endocrine pancreas. Science 210:908–910. [PubMed: 6776628]

Liu X, Xue W, Liu Q, Yu W, Fu Y, Xiong X, Ma X, Yuan Q. 2004. Swelling behaviour of alginate-chitosan microcapsules prepared by external gelation or internal gelation technology. Carbohydr Polym 56:459–464.

Machluf M 2006. Alginate–chitosan complex coacervation for cell encapsulation: Effect on mechanical properties and on long-term viability. Biopolymers 82(6):570–579. [PubMed: 16552738]

Raof NA, Mooney BM, Xie Y. 2011a. Bioengineering embryonic stem cell microenvironments for the study of breast cancer. Int J Mol Sci 12:7662–7691. http://www.pubmedcentral.nih.gov/articlerender.fcgi?artid = 3233430&tool = pmcentrez&rendertype = abstract [PubMed: 22174624]

Raof NA, Padgen MR, Gracias AR, Bergkvist M, Xie Y. 2011b. One-dimensional self-assembly of mouse embryonic stem cells using an array of hydrogel microstrands. Biomaterials 32:4498–4505. http://www.pubmedcentral.nih.gov/articlerender.fcgi?artid = 3118580&tool = pmcentrez&rendertype = abstract [PubMed: 21459438]

Rasband WS. 2004. Image processing with ImageJ. Biophotonics Int 11:36–42. http://imagej.nih.gov/ij/

Rokstad AM, Brekke O-L, Steinkjer B, Ryan L, Kolláriková G, Strand BL, Skjåk-Bræk G, Lacík I, Espevik T, Mollnes TE. 2011. Alginate microbeads are complement compatible, in contrast to

polycation containing microcapsules, as revealed in a human whole blood model. Acta Biomater 7:2566–2578. [PubMed: 21402181]

Rowley JA, Madlambayan G, Mooney DJ. 1999. Alginate hydrogels as synthetic extracellular matrix materials. Biomaterials 20:45–53. [PubMed: 9916770]

Sakai S, Inamoto K, Liu Y, Tanaka S, Arii S, Taya M. 2012. Multicellular tumor spheroid formation in duplex microcapsules for analysis of chemosensitivity. Cancer Sci 103:549–554. http://www.ncbi.nlm.nih.gov/pubmed/22168771 [PubMed: 22168771]

Schiele NR, Chrisey DB, Corr DT. 2011. Gelatin-Based laser direct-Write technique for the precise spatial patterning of cells. Tissue Eng. Part C: Methods 17:289–298. [PubMed: 20849381]

Team RC. 2014. R: A Language and Environment for Statistical Computing. R Foundation for Statistical Computing. http://www.r-project.org

Thu B, Bruheim P, Espevik T, Smidsrød O, Soon-Shiong P, Skjåk-Braek G. 1996a. Alginate polycation microcapsules. II. Some functional properties. Biomaterials 17:1069–1079. http://www.ncbi.nlm.nih.gov/pubmed/8718966 [PubMed: 8718966]

Thu B, Bruheim P, Espevik T, Smidsrød O, Soon-Shiong P, Skjåk-Bræk G. 1996b. Alginate polycation microcapsules. Biomaterials 17:1031–1040. [PubMed: 8736740]

Unser AM, Mooney B, Corr DT, Tseng Y, Xie Biomaterials Y. 2016. 3D brown adipogenesis to create "Brown-Fat-in-Microstrands." Biomaterials 75:123–134. 10.1016/j.biomaterials.2015.10.017 [PubMed: 26496384]

Wang W, Liu X, Xie Y, Zhang H, Yu W, Xiong Y, Xie W, Ma X. 2006a. Microencapsulation using natural polysaccharides for drug delivery and cell implantation. J Mater Chem 16:3252.

Wang X, Wang W, Ma J, Guo X, Yu X, Ma X. 2006b. Proliferation and differentiation of mouse embryonic stem cells in APA microcapsule: A model for studying the interaction between stem cells and their niche. Biotechnol Prog 22:791–800. http://www.ncbi.nlm.nih.gov/pubmed/16739963 [PubMed: 16739963]

Yao R, Zhang R, Lin F, Luan J. 2013. Biomimetic injectable HUVEC-adipocytes/collagen/alginate microsphere co-cultures for adipose tissue engineering. Biotechnol Bioeng 110:1430–1443. http://www.ncbi.nlm.nih.gov/pubmed/23138976 [PubMed: 23138976]

Zaytseva-Zotova DS, Udartseva OO, Andreeva ER, Bartkowiak A, Bezdetnaya LN, Guillemin F, Goergen J-L, Markvicheva E. 2011. Polyelectrolyte microcapsules with entrapped multicellular tumor spheroids as a novel tool to study the effects of photodynamic therapy. J Biomed Mater Res B Appl Biomater 97:255–262. http://www.ncbi.nlm.nih.gov/pubmed/21384545 [PubMed: 21384545]

Zhang X, Wang W, Yu W, Xie Y, Zhang X, Zhang Y, Ma X. 2005. Development of an in vitro multicellular tumor spheroid model using microencapsulation and its application in anticancer drug screening and testing. Biotechnol Prog 21:1289–1296. [PubMed: 16080713]

Zhu J, Marchant RE. 2011. Design properties of hydrogel tissue-engineering scaffolds. Expert Rev Med Devices 8:607–626. [PubMed: 22026626]

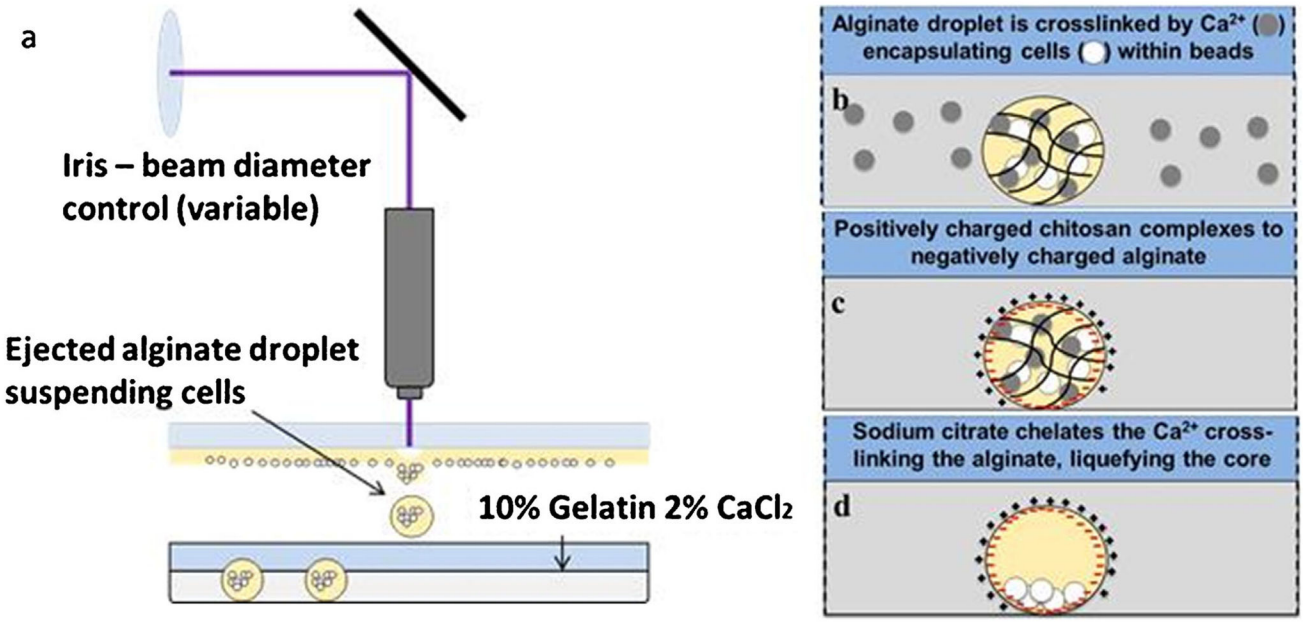

Figure 1.

Schematic depicting (**a**–**b**) microbead fabrication and (**c**–**d**) formation of capsules or microstrands. Microbeads are fabricated (**a**) using LDW to deposit alginate into (**b**) a calcium-chloride/gelatin layer, and (**c**) subsequent polyelectrolyte complex formation coats the alginate microbeads with PLL or chitosan. (**d**) The alginate is then solubilized leaving a shelled structure with an aqueous core in a precise spatial location and geometry.

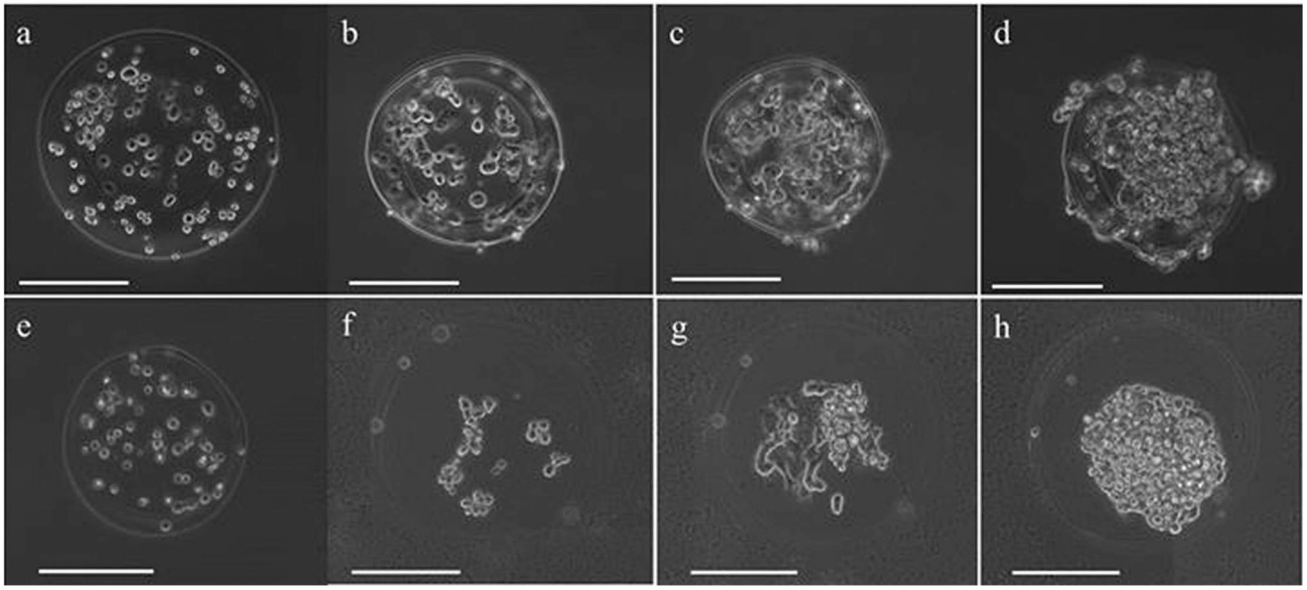

Figure 2.

Representative phase contrast images of PLL- and chitosan-coated microcapsules with M231 cell growth over 7 days. M231 cells in single PLL-coated microcapsules (**a**) immediately after capsule formation, (**b**) 1 day after capsule formation, (**c**) 3 days after capsule formation, and (**d**) 7 days after capsule formation. M231 cells in single chitosan-coated microcapsules (**e**) immediately after capsule formation, (**f**) 1 day after capsule formation, (**g**) 3 days after capsule formation, and (**h**) 7 days after capsule formation. Scale bars are 200 μm.

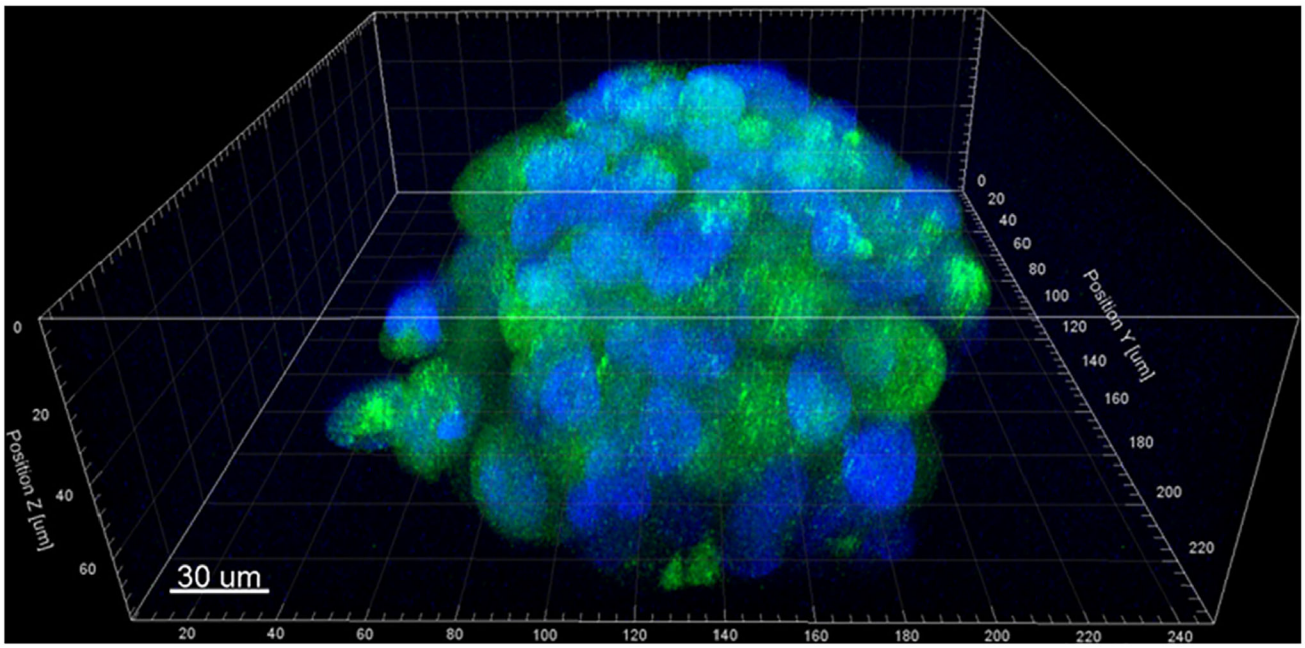

Figure 3.

Confocal image of a representative cell-loaded microcapsule at 7-days, illustrating the formation of a 3D cellular aggregate within the chitosan shell. GFP-transfected MDA-MB-231 cells (green) with DAPI-stained nuclei (blue); scale bar equals 30 μm.

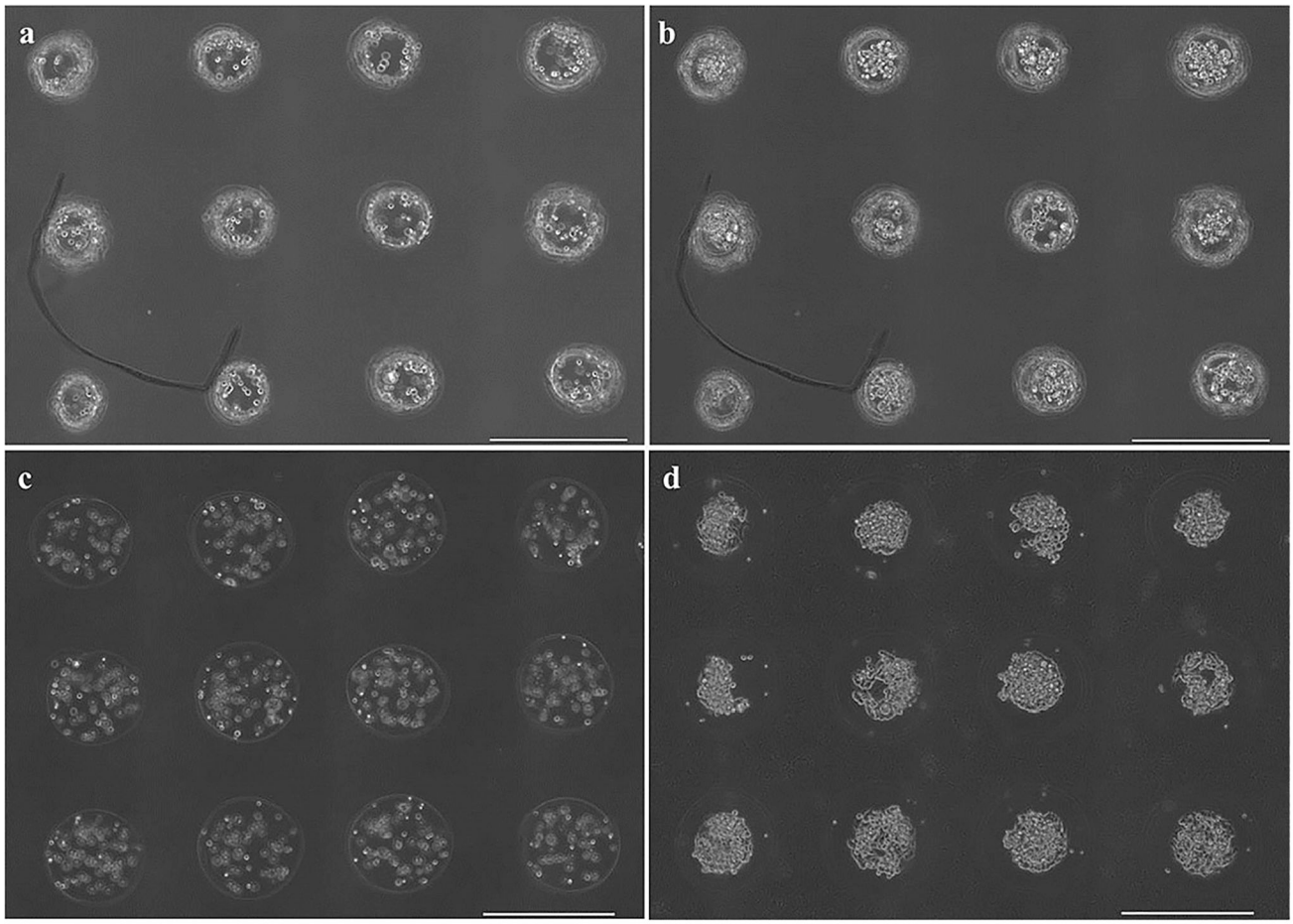

Figure 4.

3 × 4 arrays of (**a–b**) PLL-coated and (**c–d**) chitosan-coated microcapsules (**a**,**c**) immediately after capsule formation and (**b**,**d**) 5 days after capsule formation. Scale bars are 500 μm.

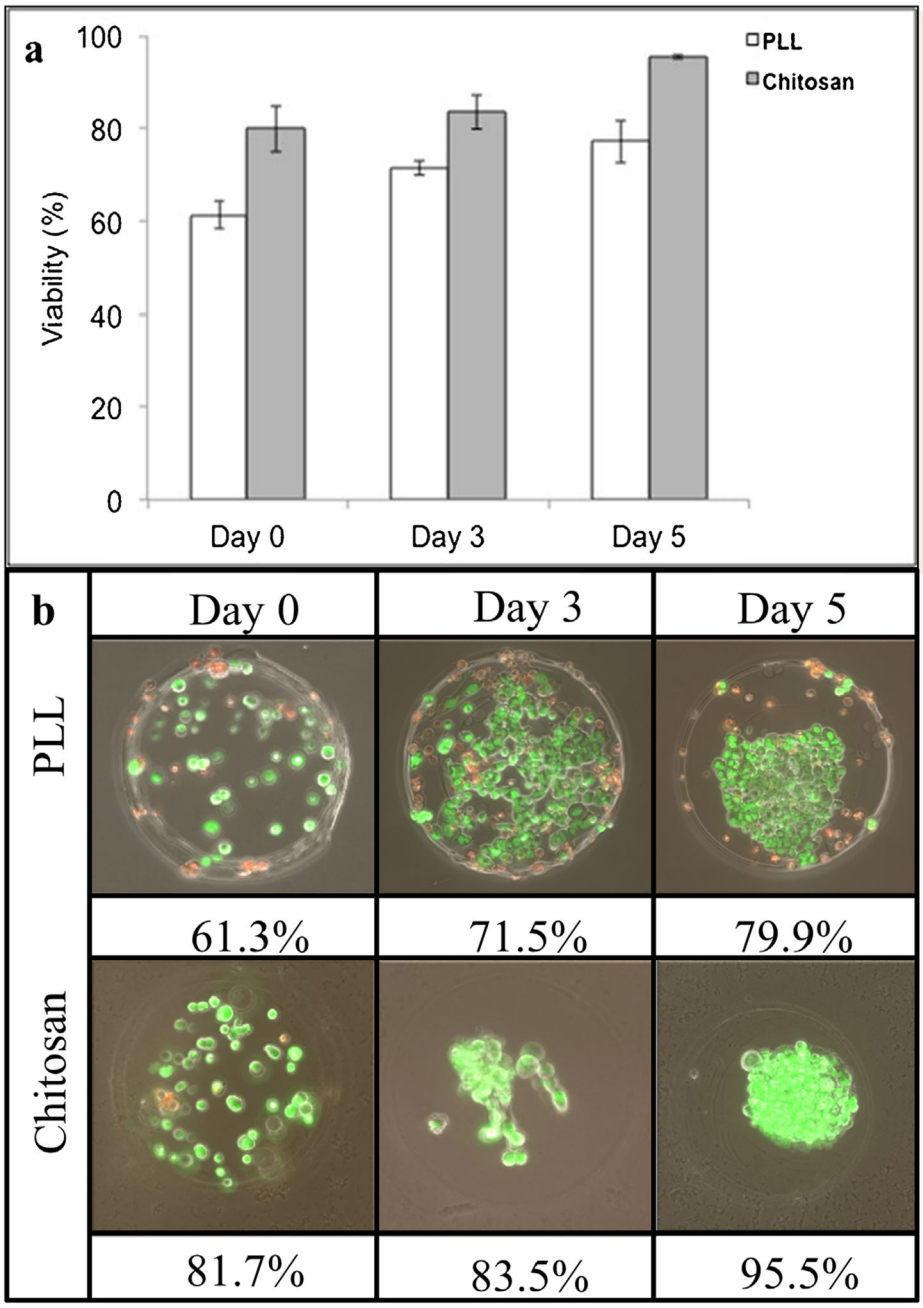

Figure 5.

Viability comparison of M231 cells in chitosan- and PLL-shelled microcapsules, over a 5-day time course. (**a**) Bar graph depiction of mean values ± standard deviation, (**b**) image set of time course with corresponding mean viability (green indicates living cells, while red indicates dead cells).

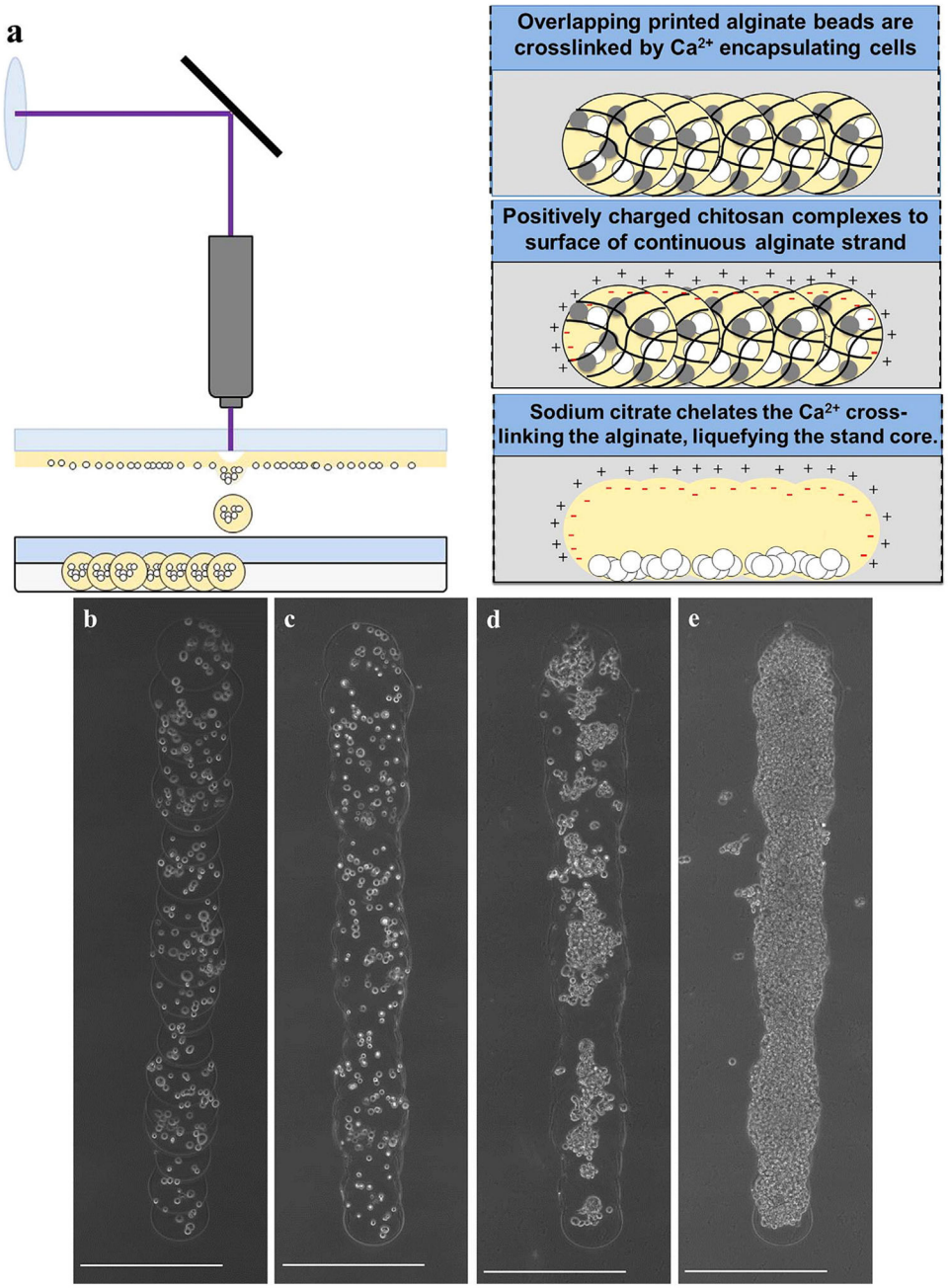

Figure 6.

(**a**) Schematic for microstrand formation by serial deposition of microbeads and subsequent processing with polymer and calcium chelator. Representative images of chitosan-microstrands, (**b**) immediately after printing, (**c**) after chitosan coating and calcium chelation resulting in a continuous strand, (**d**) 3 days in culture, and (**e**) 9 days in culture (when cells completely fill strand). Scale bars are 500 μm.

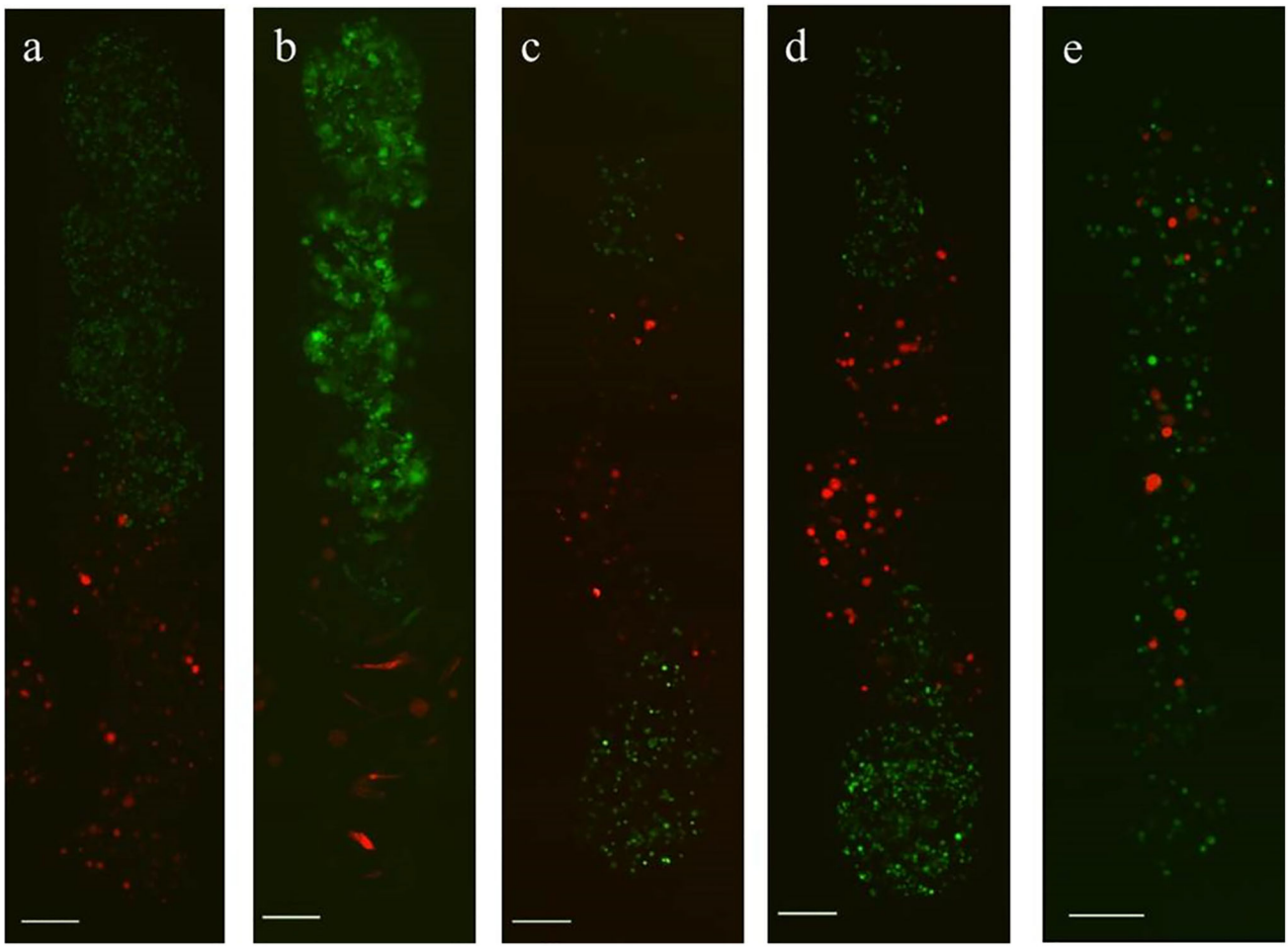

Figure 7.

Co-cultured cells within continuous chitosan-shelled microstrands, with different prescribed spatial composition. Heterogeneous microstrands of RFP fibroblasts (red) and GFP M231 (green) cells were created with three different spatial configurations: (**a–b**) microstrand with fibroblasts in one half, and M231 cells in the other at (**a**) day 0 and (**b**) day 5, resulting in segregated cell populations with a single interface between the two cell types; (**c–d**) microstrand with RFP fibroblasts in the central third of strand, and M231 cells in either end, such that there are two fibroblast-M231 interfaces between the distinct cell types, (**c**) shown immediately after creation and (**d**) after 1 day of culture; and (**e**) a microstrand in which the both cell types were printed without spatial control of the individual cell types, resulting in a more random cell distribution within the strand. Scale bars are 200 μm.

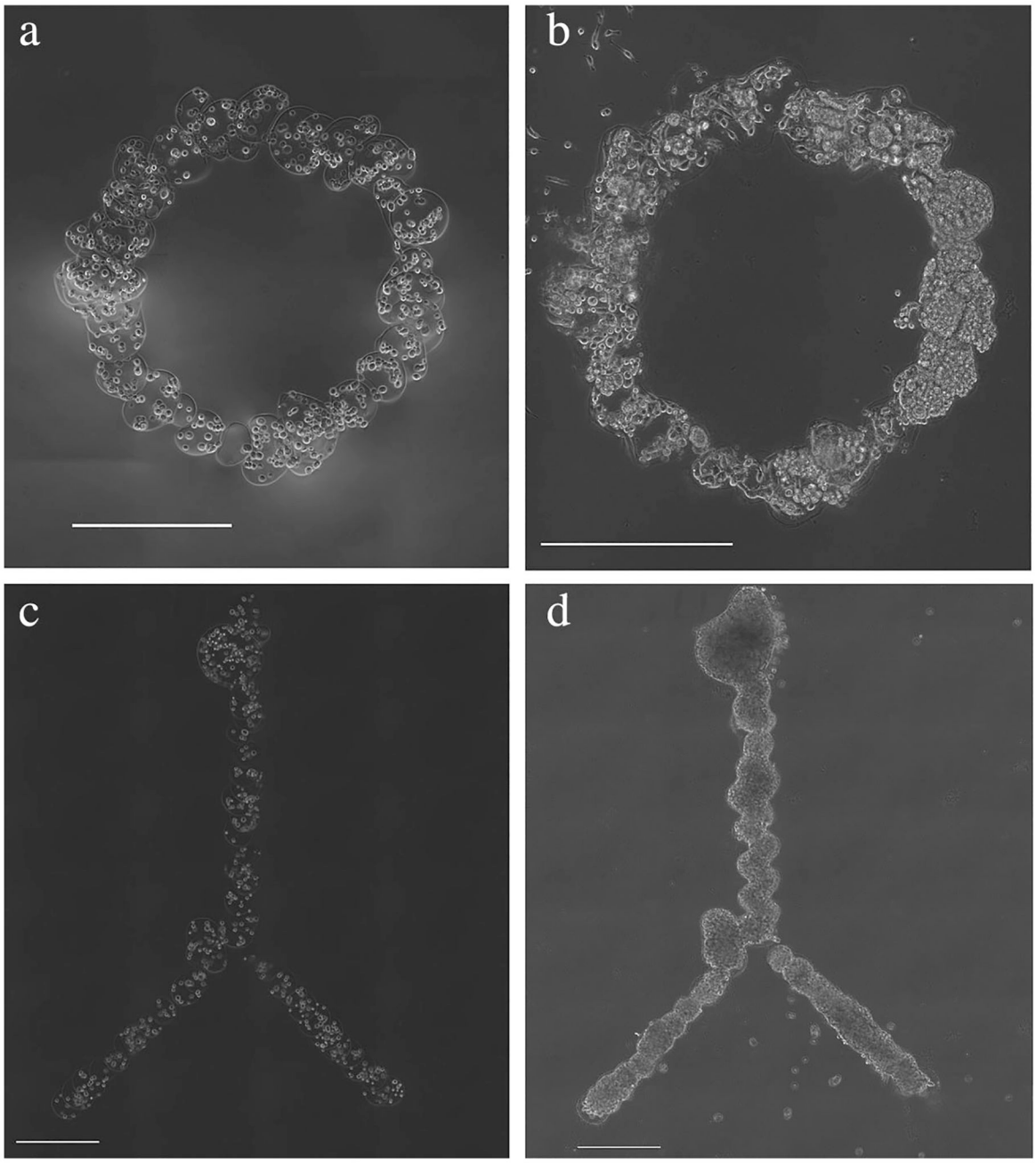

Figure 8.

Representative images of alternate geometries for shelled microstructures by serial deposition and processing of microbeads. (**a–b**) Circle and (**c–d**) bifurcation chitosan-coated structures (**a**,**c**) immediately after structure formation and (**b**,**d**) after 10 days in culture. Scale bars are 500 μm.

Table I.

Effect of polyelectrolyte coating procedure on average bead-to-bead spacing.*

	Alginate–PLL	Alginate–chitosan
Bead-to-bead spacing (μm)	612.9 ± 21.4	588.8 ± 22.8
Spacing following polycation treatment (μm)	611.0 ± 20.7	599.1 ± 27.1
Spacing change with polycation treatment (μm)	8.1 ± 7.8	9.9 ± 8.6
Diameter change with polycation treatment (%)	−6.5 ± 4.5	28.8 ± 8.5

*All patterns ($n = 3$) consisted of 12 beads printed in programmed 3 × 4 arrays with 600-μm spacing. Bead-to-bead spacing and position measurements are determined from the centroid-to-centroid distance of beads within each printed array, and then pooled for statistical analysis. Error is one standard deviation.